J. Fluid Mech. (1990), *vol.* 216, *pp.* 213–229
Printed in Great Britain

Hydrodynamic theory of glancing impact

By I. FRANKEL AND D. WEIHS
Faculty of Aerospace Engineering, Technion – Israel Institute of Technology, Haifa 32000, Israel

(Received 19 October 1988 and in revised form 17 November 1989)

Penetration of high-speed targets, such as missiles or satellites, involves a glancing impact resulting from the velocities of the target and the projectile not necessarily being parallel to one another. Glancing is different from oblique impact in that here the target is in lateral motion relative to the projectile (at speeds that may be comparable).

The effect of the transverse motion of the target on the penetration performance is analysed by means of a hydrodynamic model. As is usually done, both the projectile and target materials are taken to behave as ideal fluids, owing to the large stresses obtained upon impact. A complete description of the flow field is obtained for the planar case, making use of a transformation to the hodograph plane. Owing to the lack of symmetry, the solution is obtained indirectly from the known solution for asymmetrically impinging jets, obtaining a determinate solution by a limit process where the jet representing the target fluid becomes infinitely wide.

The variations of the rate of penetration and the streamline pattern with the respective ratios of target to projectile speeds and densities are studied. It is found that the relative lateral motion of the target causes a decrease in the rate of penetration (in comparison to normal impact). The analysis is utilized to obtain an estimate for the total depth of penetration (relative to the projectile width). Comparison with experimental data of yawed impact available in the open literature shows good agreement with the theoretical predictions when the latter are modified to account for the deceleration of a finite-length projectile.

1. Introduction

Glancing impact occurs when the target has a lateral velocity relative to the approaching projectile. Consequently their relative velocity is not parallel to the axis of the latter. (Thus 'glancing' differs from 'oblique' impact which has to do with relative direction of the projectile axis and the surface of the target.) See figure 1.

Glancing impact occurs in a number of practical penetration modes. Bless *et al.* (1978) conducted experiments on this kind of impact for yawed kinetic energy projectiles upon armour plates. In recent years the subject has attracted considerable interest as a result of the application of 'overflying top attack' mode where a shaped-charge warhead is inclined relative to the axis of the carrying missile, so as to enable a direct hit on a roof of a tank during overflight. Experimental data on the performance of such transverse shaped-charge jets were published by Golesworthy (1983) and Held (1984). Theoretical treatment of the problem (Golesworthy & Townsend 1984; Held & Fischer 1986) was, however, limited to a purely kinematic calculation of the transverse deviation of the jet particles (relative to the point of impact of the front tip of the jet) combined with semi-empirical relations for normal

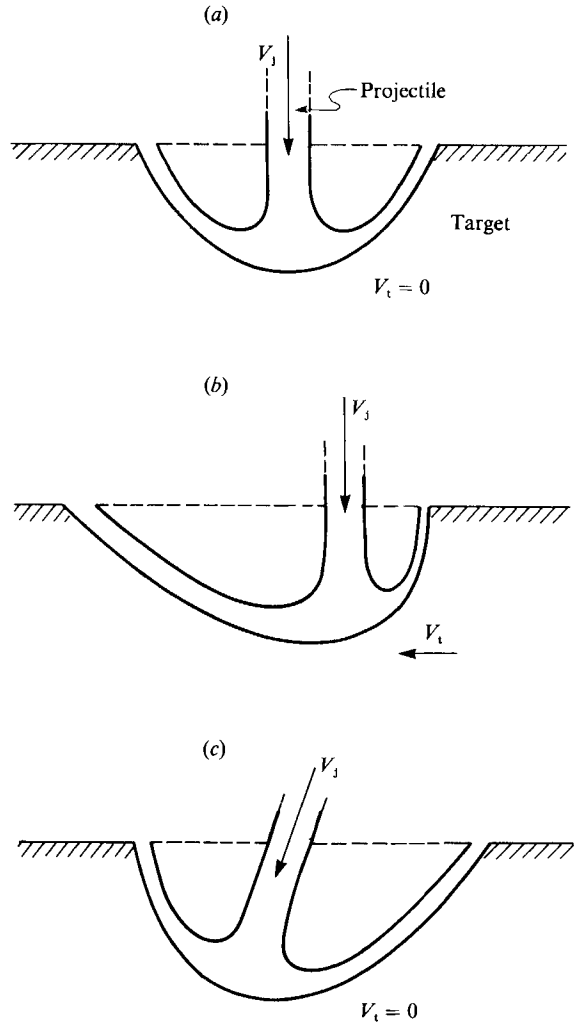

FIGURE 1 (*a*, *b*, *c*). Description of normal, glancing and oblique impacts respectively. V_j and V_t are, respectively, the projectile and target speeds.

('direct') impact. Finally, the problem is particularly important in the context of the inflight interception of missiles and satellites.

In the present study we analyse the effect of lateral target velocity on the penetration process by means of the hydrodynamic theory of impact and penetration. This was initially developed during World War II, and reported in Birkhoff *et al.* (1948) and Pack & Evans (1951). It is based on the fact that the pressures created during high-velocity impact greatly exceed the yield strengths of the materials involved, these then essentially behaving like ideal liquids. One thus neglects strength and viscosity relative to inertia effects. The penetration process well after the initial impact (when the front tip of the jet is taken to have penetrated at least several jet widths from the original surface of the target) can be approximately modelled as the quasi-steady motion of a high-velocity ideal fluid jet into an unbounded body of a quiescent fluid, both incompressible.

The model above describes the major part of the penetration process following the

impact of a 'long' projectile upon a 'thick' target (both relative to the projectile width) excluding the very beginning and the very end. The initial impact (Ravid, Bodner & Holcman 1987) produces shock waves that travel into both the target and the jet, raising the stresses well beyond the plastic limit. Hence, the present incompressible model is a useful approximation after these waves have travelled far enough (cf. Tate 1967, 1986). Plastic and spalling effects may become significant towards the end of the process owing to deceleration of the projectile or when the target is breached, respectively.

Making use of the 'free streamline' theory in conjunction with conformal mapping onto the hodograph plane (Milne-Thomson 1968, Ch. XI), Birkhoff & Caywood (1949) analysed the corresponding two-dimensional flow field. This solution was later extended by Hopkins & Robertson (1967) by means of the 'notched hodograph' which allowed for velocity variations along the free streamlines. A 'crater' of finite width was thereby obtained.

All the above applications of the hydrodynamic theory were limited to the case of normal impact, where the direction of relative motion coincides with the jet axis. In the next section this method is extended to the asymmetrical case of glancing impact. Owing to the lack of symmetry, this extension is achieved indirectly, i.e. starting from the known solution for asymmetrically impinging finite fluid jets and applying an appropriate limit process whereby the width of the jet representing the target tends to infinity. The results of the analysis are then utilized in §3 to estimate the total depth of penetration. Following Tate (1967) a modification of the theoretical predictions to account approximately for the deceleration of a finite projectile is compared to the data of Bless *et al.* (1978) obtained in reverse-impact experiments with yawed rods. Finally, §4 summarizes the main results and discusses their applicability.

2. Analysis

Applying the hydrodynamic approach outlined above, glancing impact is modelled here by a projectile jet which moves with a (vertical) velocity V_j towards the unbounded target fluid which moves transversely with the (horizontal) velocity V_t, see figure 2(*a*). Following Birkhoff *et al.* (1948), we seek to render the problem time-independent via a Galilean transformation to a frame of reference attached to the (moving) interface dividing the jet and target fluids. To this end we superpose an appropriate constant vertical velocity (of magnitude W), parallel to the jet axis. In the new frame of reference the jet and target streams appear to be advancing from infinity with the respective undisturbed speeds U_j and U_t (figure 2*b*). From the equilibrium condition at the prospective stagnation point (cf. Milne-Thomson 1968, p. 299) one obtains via Bernoulli's equation

$$\rho_t U_t^2 = \rho_j U_j^2, \tag{1a}$$

where ρ_t and ρ_j are, respectively, the target and jet densities. Consequently W satisfies the equation

$$\rho_t(V_t^2 + W^2) = \rho_j(V_j - W)^2 \tag{1b}$$

(cf. figure 2*b*). Assuming for the time being equal densities (a restriction which is relaxed later) one obtains

$$W = \tfrac{1}{2}V_j(1-\kappa^2), \quad U_j = U_t = U = \tfrac{1}{2}V_j(1+\kappa^2) \tag{2a, b}$$

where

$$\kappa = V_t/V_j. \tag{3}$$

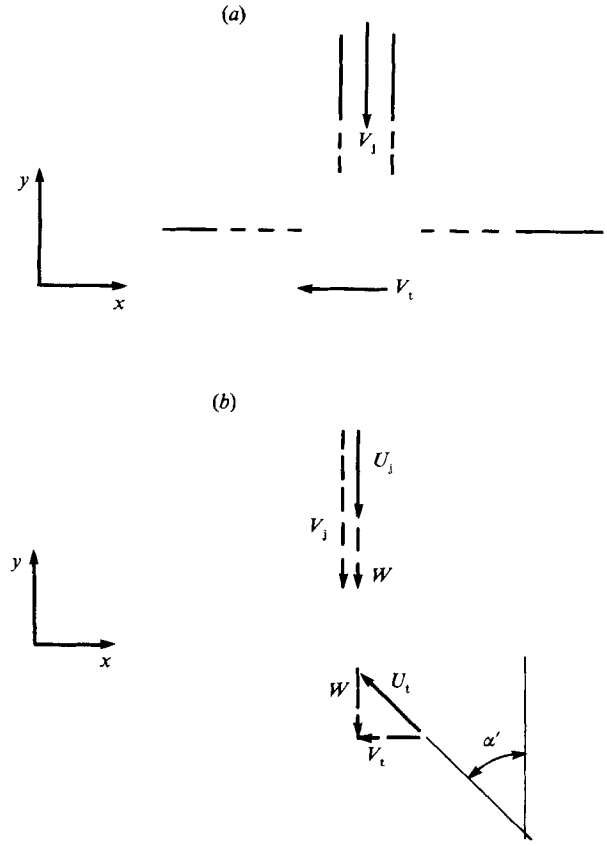

FIGURE 2. Schematic definition of speeds and directions (*a*) in a stationary frame of reference and (*b*) in a frame moving vertically downward with the constant speed W.

The velocity of the stagnation point O relative to a stationary frame of reference, is denoted by W and is equal to the rate of penetration. According to (2*a*), we note, as expected, that the transverse motion of the target reduces the rate of penetration from the classical value $\frac{1}{2}V_j$ of Birkhoff *et al.* (1948). This reduction is because successive jet particles interact with different portions of the target unlike normal impact, where they all act to deepen the same crater. The rate of penetration becomes smaller with increasing lateral target velocity, until it vanishes for $V_t = V_j$. (Even then some damage will occur on the surface of the target – 'trenching' – Bless *et al.* (1978), but this is outside the scope of the present model.)

In the plane two-dimensional case the solution will tend to the normal-impact solution of Birkhoff & Caywood (1949) as $V_t \to 0$. We therefore describe the flow field in the general ($V_t \neq 0$) case as in figure 3. Figure 3(*a*) depicts the transformed physical, $z = x + iy$, plane. The penetrator jet and the target are approaching the stagnation point O ($z = 0$) with undisturbed velocities $-iU$ and $Ue^{-i\alpha}$, respectively, where

$$\alpha = \tfrac{3}{2}\pi - \alpha', \quad \cos\alpha' = \frac{1-\kappa^2}{1+\kappa^2} \tag{4a, b}$$

(α' is defined in figure 2*b*). The value $\psi = 0$ is assigned to the dividing streamline passing through O. Along the free streamlines AC and AD, $\psi = Ul_{11}$ and $\psi = -Ul_{21}$, respectively, where l_{11} and l_{21} are the respective asymptotic distances between the

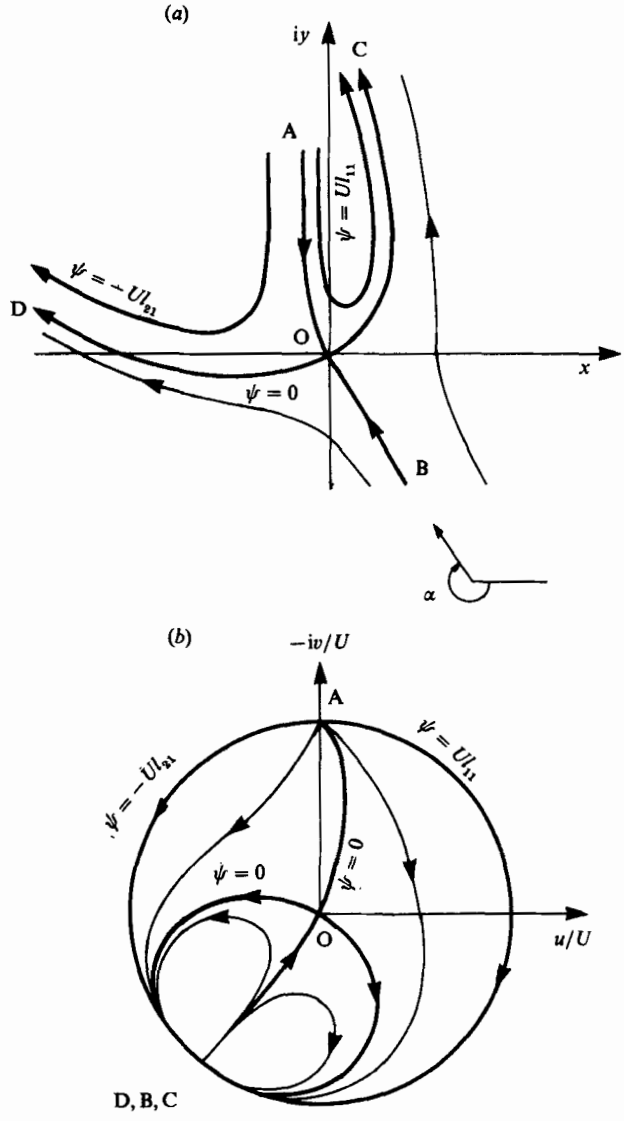

FIGURE 3. Schematic description of the flow field. (*a*) Physical $z = x+iy$ plane. (*b*) Hodograph $\omega = (u-iv)/U$ plane.

free streamlines and the dividing streamline. Since the target fluid is unbounded, we impose the 'far-field' condition that the velocities at infinity within the domain of the target (and hence within the deflected jet too) be equal to the undisturbed target velocity. Thus the velocities at C and D are also $Ue^{-i\alpha}$ (as in B).

The fluid domain is mapped in the hodograph plane of the normalized conjugate velocity, $\omega = (u-iv)/U$, into the interior of the unit circle, figure 3(*b*). The free streamlines AC and AD appear on the circumference, and the points at infinity of the target and the deflected jet (B, C and D) coincide there.

The solution of the classical problem of normal impact (by means of the mapping of half the fluid domain in both the physical z-, and the hodograph ω-planes onto the upper half of an auxiliary plane) requires the existence of a symmetry line which is

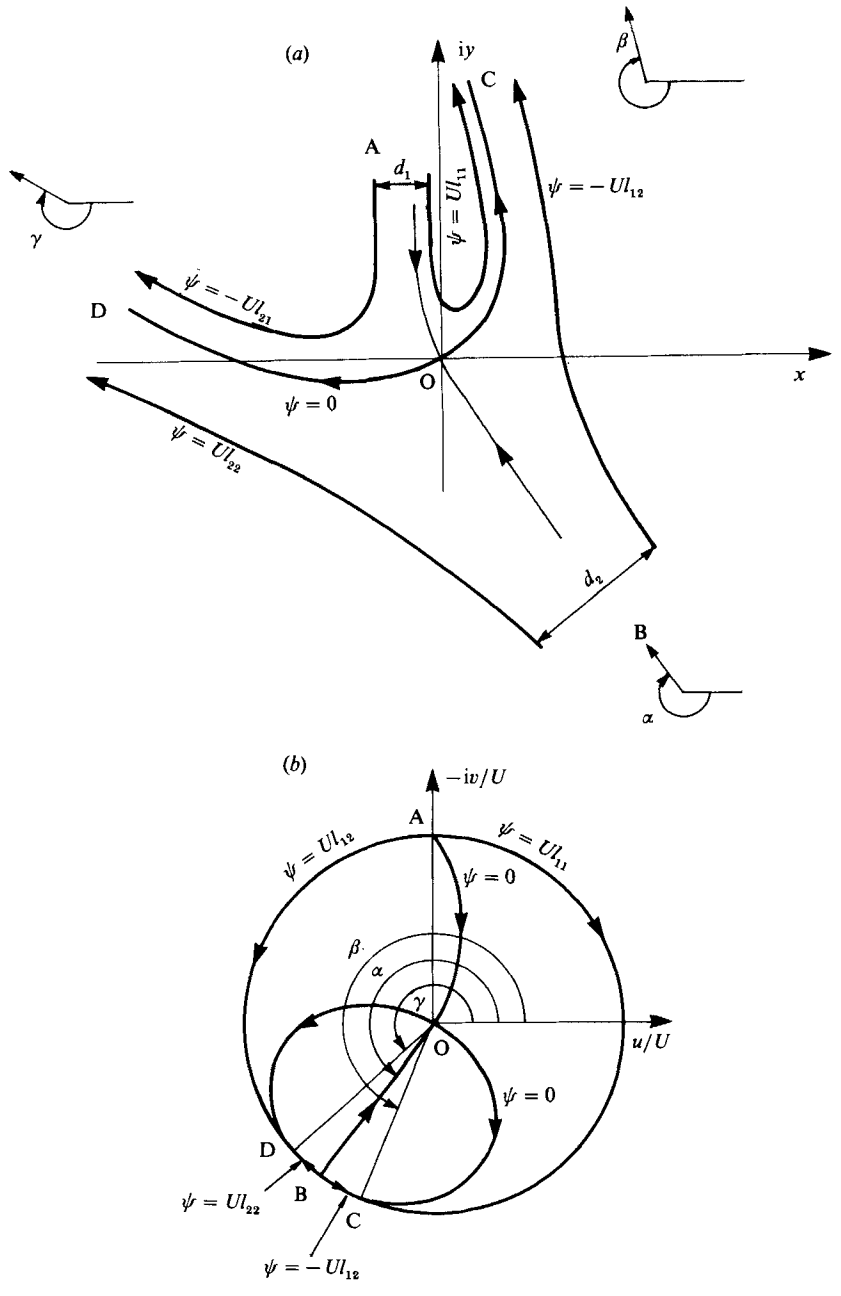

FIGURE 4. Impingement of finite jets.

a streamline (cf. figure 5*a*). The lateral motion of the target breaks this symmetry, hence the shape of the stagnation streamline (nor, in fact, any other streamline) is not given *a priori* in the present problem. Thus extension of the classical solution by means of an appropriate conformal transformation does not seem obvious.

Our approach is based instead on the known solution for the impingement of finite jets (figure 4) and the application of a suitable limit process whereby the jet representing the target fluid becomes infinitely wide. The widths of the approaching

projectile and target jets are d_1 and d_2, respectively, and their respective undisturbed velocities are $-iU$ and $U\mathrm{e}^{-i\alpha}$. The velocities at infinity of the deflected portions of the fluid are $U\mathrm{e}^{-i\beta}$ (at C) and $U\mathrm{e}^{-i\gamma}$ (at D). In addition to the free streamlines AC and AD (which have already appeared in figure 3) we now have the free streamlines BC and BD bounding the jet representing the target. Along the latter $\psi = -Ul_{12}$ and $\psi = Ul_{22}$, respectively (l_{12} and l_{22} are the analogues of l_{11} and l_{21} for the target). Here again the fluid domain is mapped onto the unit circle in the hodograph plane.

Selecting d_1 as the characteristic lengthscale, we define the non-dimensional quantities

$$l_{11} = d_1 L_{11}, \quad l_{21} = d_1 L_{21}, \quad l_{12} = \frac{d_1}{\epsilon} L_{12}, \quad l_{22} = \frac{d_1}{\epsilon} L_{22}, \tag{5a}$$

where ϵ is the ratio

$$\epsilon = d_1/d_2. \tag{5b}$$

Applying the Schwarz formula (Milne-Thomson 1968, p. 298), we express the potential as

$$f(\omega) = -\frac{1}{2\pi i}\int_{\pi/2}^{5\pi/2} \psi(\theta)\frac{\mathrm{e}^{i\theta}+\omega}{\mathrm{e}^{i\theta}-\omega}\mathrm{d}\theta. \tag{6}$$

(The limits of integration are, in general, θ_0 and $\theta_0+2\pi$, respectively, where θ_0 is an arbitrary constant. The specific choice $\theta_0 = \frac{1}{2}\pi$ is a matter of convenience). Substitution of $\psi(\theta)$ (cf. figure 4*b*) and the definitions (5*a*) and (5*b*) followed by quadratures lead to

$$\frac{\pi f(\omega)}{Ud_1} = L_{21}[\ln(1+i\omega) - \ln(1-\omega\,\mathrm{e}^{-i\gamma})] + \frac{1}{\epsilon}L_{22}[\ln(1-\omega\,\mathrm{e}^{-i\alpha}) - \ln(1-\omega\,\mathrm{e}^{-i\gamma})]$$

$$+\frac{1}{\epsilon}L_{12}[\ln(1-\omega\,\mathrm{e}^{-i\alpha}) - \ln(1-\omega\,\mathrm{e}^{-i\beta})] + L_{11}[\ln(1+i\omega) - \ln(1-\omega\,\mathrm{e}^{-i\beta})] + \tfrac{1}{2}iC. \tag{7}$$

Equation (7) is supplemented by the following conditions:
Conservation of mass yields

$$L_{11}+L_{21} = 1 \quad \text{in the projectile} \tag{8a}$$

and

$$L_{12}+L_{22} = 1 \quad \text{within the target.} \tag{8b}$$

The momentum balance parallel and perpendicular to the undisturbed target velocity results in

$$\left(L_{11}+\frac{1}{\epsilon}L_{12}\right)\cos\beta' + \left(L_{21}+\frac{1}{\epsilon}L_{22}\right)\cos\gamma' = \frac{1}{\epsilon}+\sin\alpha \tag{9}$$

and

$$\left(L_{11}+\frac{1}{\epsilon}L_{12}\right)\sin\beta' - \left(L_{21}+\frac{1}{\epsilon}L_{22}\right)\sin\gamma' = \cos\alpha \tag{10}$$

respectively, where β' and γ' are defined by

$$\beta' = \alpha+\beta', \quad \gamma = \alpha-\gamma' \tag{11}$$

respectively. Finally the constant of integration in (7) is

$$C = L_{11}(\tfrac{5}{2}\pi-\beta) - \frac{1}{\epsilon}L_{12}(\beta-\alpha) + \frac{1}{\epsilon}L_{22}(\alpha-\gamma) - L_{21}(\gamma-\tfrac{1}{2}\pi) = 0, \tag{12}$$

since the dividing streamline has been assigned the value $\psi = 0$.

Equations (8)–(10) and (12) provide altogether five equations for the six unknowns $L_{11}, L_{12}, L_{21}, L_{22}, \beta$ and γ, which is not surprising since the problem of asymmetrically impinging fluid jets is indeterminate (Milne-Thomson 1968, p. 302). However, here we are interested only in the limit of the solution when $\epsilon \to 0$. In this case it is expected that $\beta', \gamma' \to 0$ (cf. the paragraph following (4)). The asymptotic calculation (cf. Appendix A) shows indeed that β' and γ' are both $O(\epsilon^{\frac{1}{2}})$, and leads to

$$\frac{f}{Ud_1} = \frac{1}{\pi}\left\{\ln(1+\mathrm{i}\omega) - \ln(1-\omega\,\mathrm{e}^{-\mathrm{i}\alpha}) - \frac{\mathrm{i}\omega\,\mathrm{e}^{-\mathrm{i}\alpha}}{1-\omega\,\mathrm{e}^{-\mathrm{i}\alpha}}\cos\alpha + \frac{\omega\,\mathrm{e}^{-\mathrm{i}\alpha}}{(1-\omega\,\mathrm{e}^{-\mathrm{i}\alpha})^2}(1-\sin\alpha)\right\}. \quad (13)$$

As discussed in the Appendix, the limit process is singular, yet the latter result is valid throughout the finite physical plane.

Substituting (13) into the identity

$$\frac{\mathrm{d}z}{\mathrm{d}\omega} = \frac{1}{U\omega}\frac{\mathrm{d}f}{\mathrm{d}\omega}, \quad (14)$$

one obtains after quadrature

$$\frac{z}{d_1} = \frac{1}{\pi}\left\{-\mathrm{i}\ln(1+\mathrm{i}\omega) + \mathrm{i}\ln(1-\omega\,\mathrm{e}^{-\mathrm{i}\alpha}) - \mathrm{i}\frac{\omega\,\mathrm{e}^{-\mathrm{i}\alpha}}{1-\omega\,\mathrm{e}^{-\mathrm{i}\alpha}} + \frac{\omega\,\mathrm{e}^{-2\mathrm{i}\alpha}[-3+2\sin\alpha+(2-\sin\alpha)\,\omega\,\mathrm{e}^{-\mathrm{i}\alpha}]}{(1-\omega\,\mathrm{e}^{-\mathrm{i}\alpha})^2}\right\}, \quad (15)$$

where the integration constant has been selected so as to locate the stagnation point $\omega = 0$ at the origin $z = 0$. (The need for the foregoing limit process becomes clear when one attempts a 'direct' solution based on the description of the flow field in figure 3 instead of starting as above from the picture of finite jets (figure 4). This leads to an expression of $f(\omega)$ in which the non-logarithmic terms, i.e. the last two terms on the right-hand side of (13) are missing. Substitution into (14) then yields a logarithmic singularity at $\omega = 0$ in $z(\omega)$, which contradicts the assumed flow pattern (cf. figure 3). This physically unacceptable result is a consequence of an oversimplified description of the vicinity, in the hodograph plane, of the point B, C, D, one which does not satisfy conservation of momentum.)

It has been assumed in the formulation of the problem that the case of normal impact corresponds to the limit $\kappa \to 0$. This limit is represented by $\alpha = \frac{3}{2}\pi$ (cf. (4)). Substitution of this value into (13) and (15) yields

$$\frac{f}{Ud_1} = \frac{1}{\pi}\left[\ln(1+\mathrm{i}\omega) - \ln(1-\mathrm{i}\omega) - \frac{2\mathrm{i}\omega}{(1-\mathrm{i}\omega)^2}\right] \quad (16)$$

and

$$\frac{z}{d_1} = \frac{1}{\pi}\left[-\mathrm{i}\ln(1+\mathrm{i}\omega) + \mathrm{i}\ln(1-\mathrm{i}\omega) + \frac{2\omega(3-2\mathrm{i}\omega)}{(1-\mathrm{i}\omega)^2}\right] \quad (17)$$

respectively. A reversal of the direction of the streamlines and a $\frac{1}{2}\pi$ rotation of the frame of reference readily demonstrate that (16) and (17) revert to the results of Birkhoff & Caywood (1949, their equations (3)–(5)) as well as those of Hopkins & Robertson (1967, their equations (5) and (7) in the limit $K \to 1$).

A complete description of the penetration process is provided by the streamline pattern (in particular the dividing streamline and the free streamlines) in conjunction with the rate of penetration, W. Figures 5(*a*)–5(*d*) describe the dependence of this streamline pattern upon α (or the velocity ratio κ, equation (4)) by depicting it in

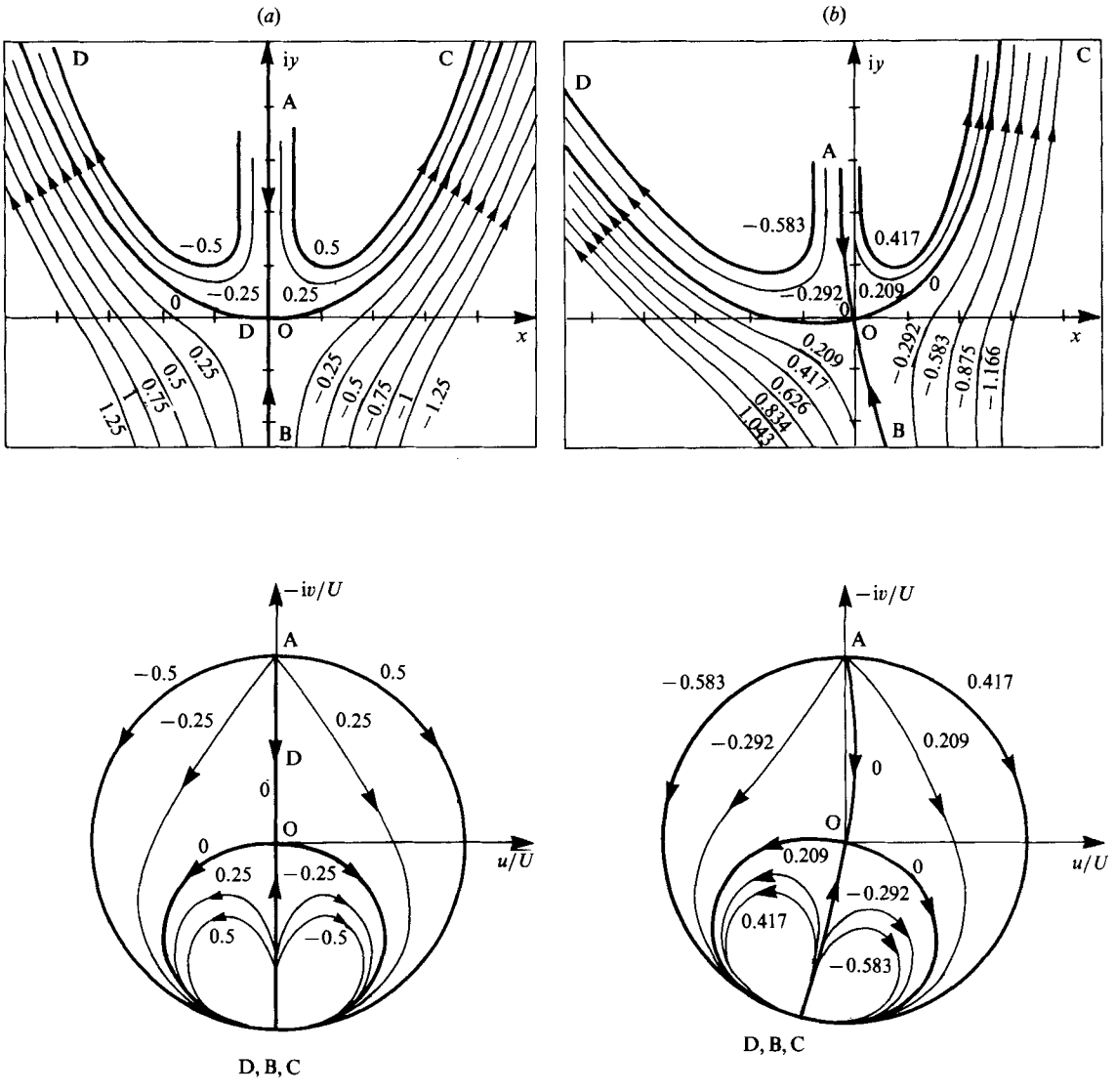

FIGURE 5(*a*, *b*). For caption see next page.

both the physical and hodograph planes for $\alpha/\pi = \frac{3}{2}, \frac{17}{12}, \frac{4}{3}$ and $\frac{7}{6}$, i.e. velocity ratios of $\kappa = 0$, 0.132, 0.268, 0.577, respectively. (The flow fields corresponding to $\alpha = 3\pi/2 \pm \alpha'$ are obtainable as mirror images of each other, consequently the variation is considered only for $\alpha \leqslant 3\pi/2$.) The picture becomes increasingly asymmetric with decreasing values of α.

As a consequence of the 'far-field' conditions in the present problem, the 'windward' portion of the deflected fluid inevitably intersects the oncoming jet for any $\alpha < 3\pi/2$. (This is particularly evident in figure 5*d*.) In the foregoing solution these crossing streams do not interfere with each other, since they take place on different sheets of a Riemann surface. (A similar phenomenon was discussed by Lighthill 1979.) Potential implications of this intersection on the applications of this model will be discussed in the next section.

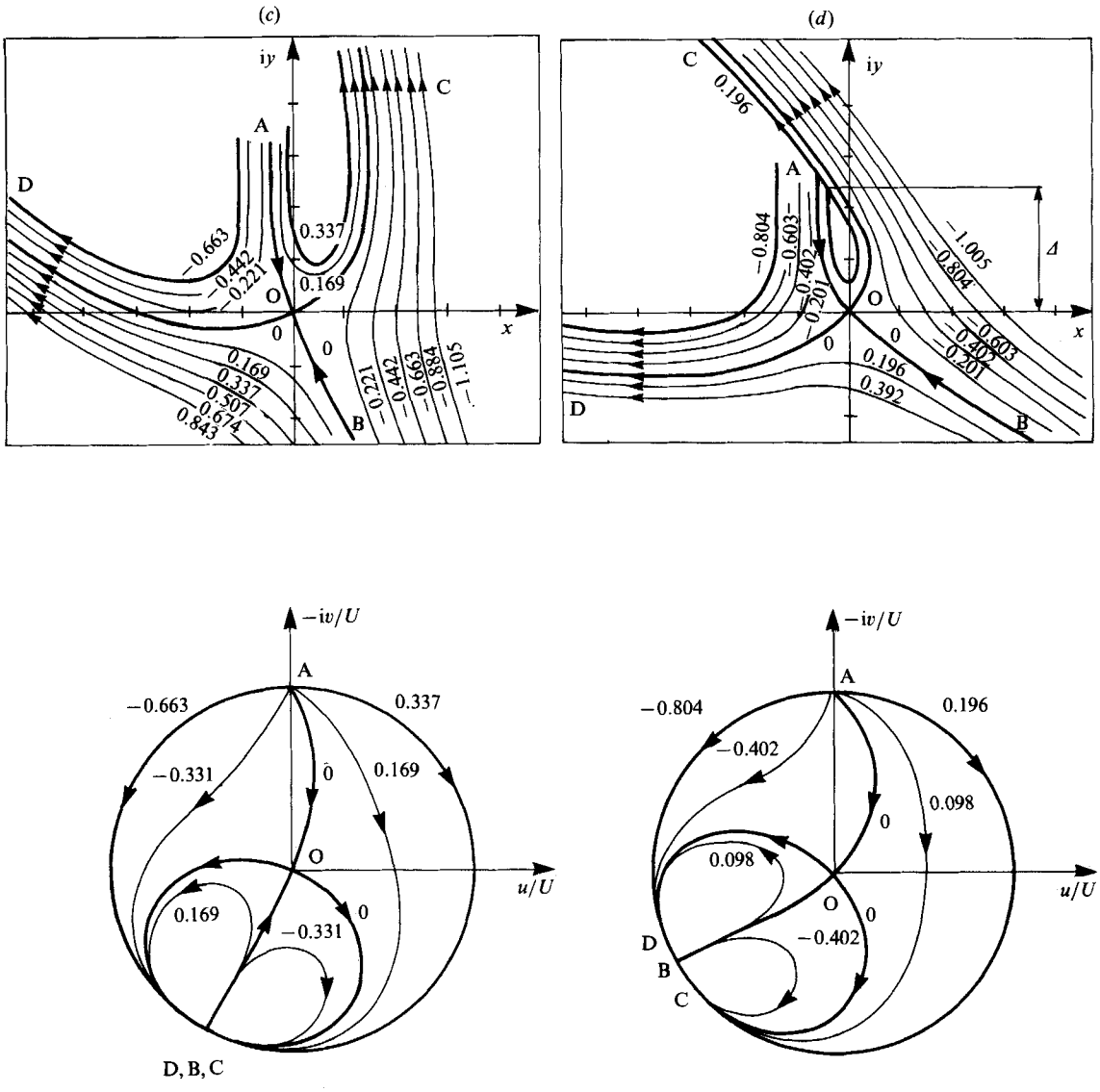

FIGURE 5. Variation of flow pattern with α: (*a*) $\alpha/\pi = \frac{3}{2}$, (*b*) $\frac{17}{12}$, (*c*) $\frac{4}{3}$, (*d*) $\frac{7}{6}$. (The numbers indicate the corresponding values of the non-dimensional stream function, ψ/Ud_1.)

2.1. *Unequal densities*

We now extend the foregoing analysis to the case when the respective densities of the jet and the target, ρ_j and ρ_t, are not necessarily equal. Consider first the rate of penetration, W, which satisfies

$$(1-\lambda)\left(\frac{W}{V_j}\right)^2 - 2\frac{W}{V_j} + (1-\lambda\kappa^2) = 0 \tag{18}$$

(which is (1*b*) recast in non-dimensional form), where

$$\lambda = \rho_t/\rho_j. \tag{19}$$

Considering the respective limits $\lambda \to 1$ and $\kappa \to 0$ we see that the solution that is compatible with the present problem is

$$W = (1-\lambda)^{-1}\{1-\lambda^{\frac{1}{2}}[1+(1-\lambda)\kappa^2]^{\frac{1}{2}}\}V_j. \tag{20}$$

Thus W can be readily verified as decreasing monotonically with increasing λ and κ from the value $W = V_j$ for $\lambda = 0$ (which corresponds to the unopposed motion of the jet into vacuum).

(For $\lambda > 1$ and $\kappa > \kappa_1 = (\lambda-1)^{-\frac{1}{2}}$, (18) possesses no real solutions, because there exists no inertial frame of reference where the flow appears steady. This, however, does not restrict the applicability of the present analysis, because W is already negative (no penetration) for $\kappa = \kappa_2 = \lambda^{-\frac{1}{2}}$.)

The solution of the kinematic problem, (13) and (15), and hence the streamline pattern are unaffected by the variation of λ, but the fluid velocities are now normalized by

$$U_j = V_j - W = \lambda^{\frac{1}{2}}(1-\lambda)^{-1}\{[1+(1-\lambda)\kappa^2]^{\frac{1}{2}}-\lambda^{\frac{1}{2}}\}V_j \tag{21a}$$

in the jet domain, whereas in the target domain they are normalized by

$$U_t = \lambda^{-\frac{1}{2}}U_j = (1-\lambda)^{-1}\{[1+(1-\lambda)\kappa^2]^{\frac{1}{2}}-\lambda^{\frac{1}{2}}\}V_j. \tag{21b}$$

In particular the dividing streamline becomes a 'slip line' across which the respective fluid speeds in the jet and target, q_j and q_t, are related by

$$q_j = \lambda^{\frac{1}{2}}q_t.$$

This assures, via Bernoulli's equation, the continuity of pressures across the dividing streamline. The angle α' is now

$$\cos\alpha' = \frac{W}{U_t} = \frac{1-\lambda^{\frac{1}{2}}[1+(1-\lambda)\kappa^2]^{\frac{1}{2}}}{[1+(1-\lambda)\kappa^2]^{\frac{1}{2}}-\lambda^{\frac{1}{2}}} \tag{22}$$

instead of (4*b*). Equation (4*a*) relating α and α' remains the same. Thus while the dependence of the flow pattern upon α (figures 5(*a*)–5(*d*)) is unchanged, its variation with κ is modified by variations in λ.

3. Depth of penetration

Experimental data (Golesworthy 1983; Held 1984) regarding glancing impact of shaped-charge jets indicate that, owing to the transverse motion of the target, the jet may eventually contact the side of the crater. When this occurs the rest of the jet is used up through interaction with the wall or causes superficial damage on the surface of the target (trenching), but does not deepen the crater any further (Held & Fischer 1986).

We thus distinguish between two cases: I the entire length of the jet contributes to penetration; II the depth of penetration is limited by the aforementioned interaction with the crater wall.

Define Δ as the vertical (parallel to the undisturbed jet axis) coordinate of the point where the 'windward' branch of the free streamline crosses itself (see figure 5*d*). Our estimate of the total penetration depth relates the transition from case I to case II to Δ: since the interaction with the wall of the crater will not take place much above the original level of the free surface of the target, we assume that case II occurs when the projectile has penetrated a distance Δ and the remaining segment of the jet at that instant is longer than Δ.

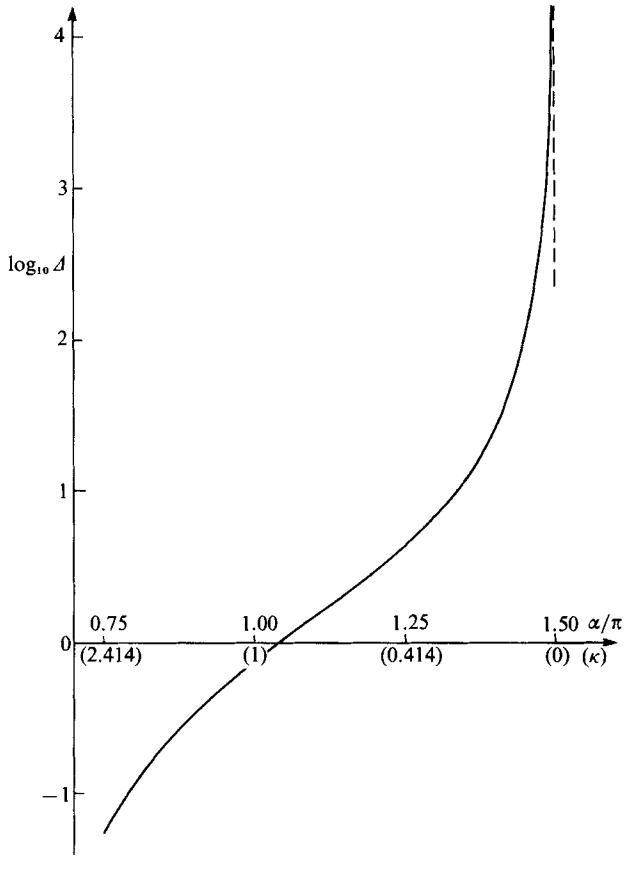

FIGURE 6. Variation of $\log_{10}\Delta$, the logarithm of the vertical coordinate of the point where the 'windward' branch of the free streamline crosses itself, with the glancing angle α (or with the speed ratio κ when the density ratio is $\lambda = 1$).

Thus the total penetration is here estimated as

$$\delta \leqslant \min\left\{\frac{W}{U_j}L, \left(1+\frac{W}{U_j}\right)\Delta\right\} \tag{23}$$

where L is the aspect ratio (length to width) of the projectile. The terms $(W/U_j)L$ and $(W/U_j)\Delta$ are obtained by the product of the penetration rate W and the duration of the interaction, L/U_j and Δ/U_j, respectively, until the corresponding jet segment is used up. From (2a, b), (20) and (21a)

$$\frac{W}{U_j} = \begin{cases} \dfrac{1-\kappa^2}{1+\kappa^2} & \text{for } \lambda = 1 \\ \dfrac{1-\lambda^{\frac{1}{2}}[1+(1-\lambda)\kappa^2]^{\frac{1}{2}}}{\lambda^{\frac{1}{2}}\{[1+(1-\lambda)\kappa^2]^{\frac{1}{2}}-\lambda^{\frac{1}{2}}\}} & \text{for } \lambda \neq 1. \end{cases} \tag{24}$$

Figure 6 displays the variation of Δ with α in the interval $3\pi/4 \leqslant \alpha < 3\pi/2$ on a logarithmic scale (also shown are the corresponding values of κ for $\lambda = 1$). Δ grows monotonically with α and becomes infinitely large when $\alpha \to 3\pi/2$ (in which case there

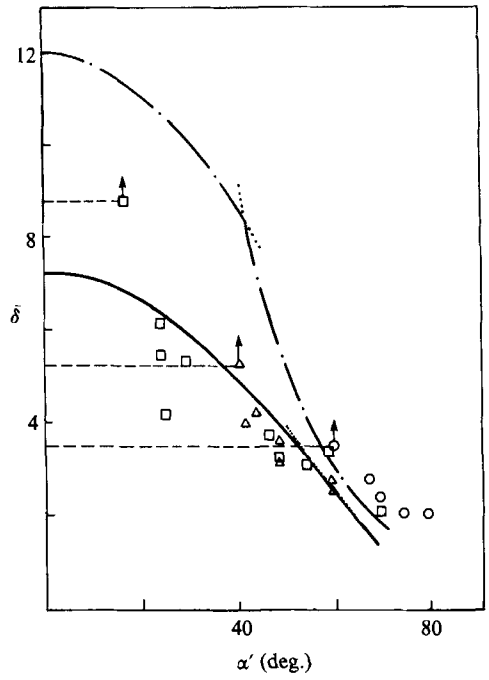

FIGURE 7. Variation of $\bar{\delta}$ the total (non-dimensional) penetration depth (perpendicular to the target surface) with the angle α' for rods of aspect ratio $L = 11.7$. –·–·–, equation (23); ——, the modified theoretical estimate which incorporates the deceleration of the rods. Also shown are the experimental data of Bless *et al.* (1978) for rods of diameter 1.47 mm (□), 2.47 mm (△) and 3.68 mm (○). The horizontal broken lines mark the respective non-dimensional penetration depths corresponding to perforations of the 12.7 mm target plates, and the values of α' below which they were observed.

is no intersection). When $\alpha \approx 1.2\pi$ (corresponding to $\kappa \approx 0.510$ for $\lambda = 1$), $\Delta \approx 3$. For smaller values of α the total depth of penetration becomes vanishingly small. Furthermore, it becomes questionable whether the present quasi-steady view is still a justifiable approximation. Hence the range of engineering applicability of the present analysis is estimated as $1.2\pi \leqslant \alpha \leqslant 1.5\pi$.

The predictions based on the present analysis are compared in the following with the data of Bless *et al.* (1978). These were obtained in 'reverse-impact' experiments. Steel (R. H. A.) target plates were launched perpendicularly to their respective planes at $U_0 \approx 2.15$ km/s against fixed steel (SAE 4340) rods of aspect ratio 11.7 whose axes were inclined at a yaw angle θ to the velocity of the plates. This yaw angle is related to the glancing speed ratio κ via

$$\tan\theta = \kappa \tag{25}$$

hence (for $\lambda = 1$)

$$\alpha' = 2\theta. \tag{26}$$

Figure 7 presents the variation of the non-dimensional depth of penetration perpendicular to the surface of the target, $\bar{\delta}(= \delta\cos\theta)$ with α' for rods of aspect ratio $L = 11.7$. The dot-dash line corresponds to the theoretical estimate, (23). The transition from case I to case II takes place at $\alpha' \approx 41.5°$. Equation (23) is expected to overestimate the total depth of penetration because: (i) It is based in part on a two-dimensional model whereas the experimental configuration of Bless *et al.* (1978) is three-dimensional. (ii) In finite-length rods, the rear portion of the projectile is

decelerated owing to the axial pressure distribution, thus reducing its contribution to penetration.

The former effect is discussed in the next section. In the following, the theoretical estimate is modified to account approximately for the latter effect by calculating the deceleration of the projectile during the penetration process. This calculation is based on the modified hydrodynamic theory (Eichelberger 1956; Tate 1967) which assumes that the projectile and target materials flow hydrodynamically only when certain pressures, Y_p and R_t, respectively, are exceeded. Following Tate (1967), the equation of motion is written for the rear (rigid) portion of the rod. This is then combined with the kinematic relation between the respective projectile and penetration speeds and the rate of consumption of the rod, and a 'modified Bernoulli's equation' which incorporates the constants Y_p and R_t. Taking the values suggested by Tate (1967), i.e. the Hugoniot elastic limit (15 kbar for SAE4340) and the ratio $R_t/Y_p = 3.5$ (for steel–steel impact) we obtain after some algebraic manipulation the results represented by the full line in figure 7. (This calculation is not inconsistent with the quasi-steady model assumed here. The results (Tate 1967) show that almost all of the penetration is achieved before any substantial deceleration of the projectile takes place.) It is interesting to note that, owing to the deceleration, the transition to case II occurs only at $\alpha' \approx 54°$ and even then the difference between the two cases remains small.

Along with the foregoing theoretical predictions, figure 7 presents the experimental data of Bless *et al.* (1978) for rods of aspect ratio $L = 11.7$ and diameters of 1.47 mm (squares), 2.47 mm (triangles) and 3.68 mm (circles) (the empirical correlations included in the original reference have been omitted here). When the range of higher values of $\alpha' (> \sim 0.3\pi)$ is excluded (cf. the description of figure 6), it seems as if the modified theoretical prediction (the full line) is still an overestimate. One should note, however, that the experimental data presented result in a somewhat biased picture because they contain only the cases of non-perforations. Since the experiments were performed with target plates whose maximal thickness was 12.7 mm, it was impossible to measure penetration depth which exceeded the values $\bar{\delta} = 8.64$, 5.14 and 3.45 for the three respective rod diameters. According to additional data published by Bless *et al.* (1978), perforations of the 12.7 mm target plates were observed for yaw angles corresponding to α' of less than 16°, 40° and 60°, respectively. Had thicker target plates been used in the experiments, additional data points would have appeared above the three respective horizontal broken lines. The modified theoretical estimate is thus seen to yield a good agreement with the available experimental data.

4. Concluding remarks

The hydrodynamic theory of impact and penetration has been extended to cases of glancing impact. Retaining the usual dynamic assumptions of the hydrodynamic theory, a quasi-steady description is obtained via a transformation to a frame of reference that moves with the penetration velocity. The penetration velocity W is determined from the dynamic condition on the dividing surface between the projectile and target materials. The resulting expressions (2*a*) and (20) show that the lateral motion of the target reduces the rate of penetration. An important feature of these results is their validity in three-dimensional geometries.

A complete description of the flow field is obtained for planar two-dimensional flows through application of the hodograph transformation. Owing to the lack of

symmetry in glancing situation, we start with the known solution for asymmetrically impinging fluid jets and the problem is scaled with respect to the projectile width. We then apply a limit process whereby the width of the jet representing the target tends to infinity. This, in conjunction with the appropriate 'far-field' conditions, results in a unique limit solution in spite of the well-known indeterminacy of the original problem. The solution is valid throughout the finite physical plane although the limit process is singular.

The analysis is generalized to cases where the density ratio is $\lambda \neq 1$. The kinematic problem of determining the complex potential, f, and the physical coordinate, z, as functions of the conjugate velocity ω is unaffected by λ, hence the expressions for $f(\omega)$ and $z(\omega)$, (13) and (15) respectively, remain valid. Consequently, for a given value of glancing angle α the streamline pattern remains the same. The relation between α and the speed ratio κ is, however, modified by λ and the fluid velocities are now normalized relative to different speeds in the projectile and target domains, U_t and U_j, (21a) and (21b) respectively. In particular the dividing streamline becomes a slip line thus assuring equality of pressures across it.

The results of the analysis are used to predict the depth of penetration obtained for finite projectiles. A distinction is made between the two cases: I the whole length of the rod contributes to the penetration; II the total depth is limited by the interaction with the wall of the crater (resulting from the lateral target motion).

A by-product of this finite-penetrator calculation is a lower bound ($\alpha > \sim 1.2\pi$) on the values of α for which the present quasi-steady model is expected to apply. The theoretical prediction, (23), is expected to overestimate the depth of penetration because of the finite length of the projectile and the three-dimensionality of the experimental configuration of Bless *et al.* (1978). The former effect has been treated approximately through a modified calculation following Tate (1967) which incorporated the deceleration of the projectile. While this modification seems sufficient to yield a good agreement with the experimental data (figure 7), the role of three-dimensionality nevertheless deserves some further comment.

It is important to note that our estimate corresponding to case I is unaffected by three-dimensionality, because, as mentioned above, W is not. On the other hand, a three-dimensional jet will create a narrower crater within the target which will result in a lower value of Δ for a given α. This will lower the curve corresponding to case II in figure 7 and will shift the transition from case I to case II to a lower value of α'. A quantitative estimate of these trends requires a fully three-dimensional numerical solution, which constitutes a possible extension to the present work. For the present combination of parameters corresponding to the yawed-impact experiments of Bless *et al.* (1978), case I, however, covers most of the relevant range of α' which in turn may explain the good agreement observed in figure 7 between the modified theoretical predictions and the (three-dimensional) experimental results.

Appendix. The asymptotic result, equation (13)

Algebraic manipulation of (8)–(12) yields the equation

$$\sin\beta' + \sin\gamma' + \epsilon\cos\alpha(\cos\gamma' - \cos\beta') + \epsilon\sin\alpha(\sin\beta' + \sin\gamma') = (1+\epsilon)\sin(\beta'+\gamma') \quad (A\ 1)$$

from which it follows that

$$\beta' \approx \beta_0\epsilon^{\frac{1}{2}} + O(\epsilon), \quad \gamma' \approx \gamma_0\epsilon^{\frac{1}{2}} + O(\epsilon), \qquad (A\ 2a, b)$$

where

$$\beta_0\gamma_0 = 2(1-\sin\alpha). \qquad (A\ 2c)$$

(From (9) and (10) in conjunction with the fact that L_{11}, L_{12}, L_{21} and L_{22} are all $O(1)$, one readily concludes that β' and γ' being both $O(\epsilon^{\frac{1}{2}})$ for $\epsilon \to 0$ is the only consistent choice.) We then proceed by expanding the terms $\ln(1-\omega e^{-i\gamma})$ and $\ln(1-\omega e^{-i\beta})$ in power series of $(1-e^{i\gamma'})$ and $(1-e^{-i\beta'})$, respectively. When these are substituted into (7) we obtain

$$\begin{aligned}\frac{\pi f}{Ud_1} \approx{}& \ln(1+i\omega)-\ln(1-\omega e^{-i\alpha})-(1-\sin\alpha+i\cos\alpha)\frac{\omega e^{-i\alpha}}{1-\omega e^{-i\alpha}}\\ &+\frac{1}{2}\left(\frac{\omega e^{-i\alpha}}{1-\omega e^{-i\alpha}}\right)^2\left[\left(L_{21}+\frac{1}{\epsilon}L_{22}\right)(1-e^{i\gamma'})^2+\left(L_{11}+\frac{1}{\epsilon}L_{12}\right)(1-e^{-i\beta'})^2\right]\\ &-\frac{1}{3}\left(\frac{\omega e^{-i\alpha}}{1-\omega e^{-i\alpha}}\right)^3\left[\left(L_{21}+\frac{1}{\epsilon}L_{22}\right)(1-e^{i\gamma'})^3+\left(L_{11}+\frac{1}{\epsilon}L_{12}\right)(1-e^{-i\beta'})^3\right]+\dots\\ &+\frac{(-1)^n}{n}\left(\frac{\omega e^{-i\alpha}}{1-\omega e^{-i\alpha}}\right)^n\left[\left(L_{21}+\frac{1}{\epsilon}L_{22}\right)(1-e^{i\gamma'})^n+\left(L_{11}+\frac{1}{\epsilon}L_{12}\right)(1-e^{-i\beta'})^n\right]+\dots,\end{aligned} \tag{A 3}$$

where the zeroth- and first-order terms have been expressed by making use of the conservation of mass, (8), and conservation of momentum, (9) and (10), respectively. In order to express the higher-order terms one needs to make use of (A 2). A tedious calculation then leads to

$$\begin{aligned}\frac{\pi f}{Ud_1} \approx{}& \ln(1+i\omega)-\ln(1-\omega e^{-i\alpha})-\frac{i\omega e^{-i\alpha}}{1-\omega e^{-i\alpha}}\cos\alpha-\frac{\omega e^{-i\alpha}}{(1-\omega e^{-i\alpha})^2}(1-\sin\alpha)\\ &+O\left\{\frac{\epsilon^{\frac{1}{2}}}{(1-\omega e^{-i\alpha})^3},\frac{\epsilon}{(1-\omega e^{-i\alpha})^4},\dots,\frac{\epsilon^{n/2}}{(1-\omega e^{-i\alpha})^{n+2}},\dots\right\}.\end{aligned} \tag{A 4}$$

The indeterminateness of the problem allows for some freedom in the choice of the specific limit process. Assuming $\beta' = \gamma'$ when $\epsilon \to 0$, the error terms in (A 3*a*, *b*) are both reduced to $O(\epsilon^{\frac{3}{2}})$ and the odd error terms containing the fractional powers of ϵ are removed from the right-hand side of (A 4). There is no way to eliminate the rest of the (even) error terms and thus the expansion (A 4) is non-uniform at the point B, $\omega = e^{i\alpha}$, in the hodograph plane (see figure 4). The asymptotic result, (13), is thus valid outside the neighbourhood

$$\omega - e^{i\alpha} \approx O(\epsilon^{\frac{1}{4}}) \tag{A 5}$$

of the point B. (In fact $|\omega - e^{i\alpha}| \gg \epsilon^{\frac{1}{2}}$ is sufficient to assure the validity of the asymptotic expansion (A 4). The stronger requirement embodied in (A 5) is necessary to guarantee the actual vanishing of the error terms.) When (A 5) is substituted into (15) we see that the non-uniformity is confined to the vicinity

$$z \approx O(\epsilon^{-\frac{1}{2}}) \tag{A 6}$$

of the point of infinity on the sheet which contains the target and deflected jet fluid on the Riemann surface which represents the solution. We thus conclude that (13) and (15) resulting from the limit process

$$\epsilon \to 0, \omega \neq e^{i\alpha} \quad \text{(fixed)} \tag{A 7}$$

are valid throughout the finite physical plane.

The singularity in the limit process is because for all $\epsilon > 0$ (however small) the original problem contains an additional couple of free streamlines (which disappear only for $\epsilon = 0$). Thus the non-uniformity of the expansion (A 4) results from its inability to satisfy the suitable boundary conditions on these additional free streamlines. As $\epsilon \to 0$ these streamlines become farther removed away from the domain of interest in the physical plane. Furthermore, as a consequence of the far-field conditions imposed in the analysis, the fluid velocity when approaching the target infinity deviates only slightly from the unperturbed velocity, $U e^{i\alpha}$. Thus when $\epsilon \to 0$ the streamlines near the target infinity become in fact 'almost free' streamlines. Therefore the small error introduced here in satisfying the conditions at infinity has only local influence on the solution and does not affect the validity of (13) and (15).

REFERENCES

Birkhoff, G. & Caywood, T. E. 1949 Fluid flow patterns. *J. Appl. Phys.* **20**, 646–659.

Birkhoff, G., MacDougal, D. F., Pugh, E. M. & Taylor, G. I. 1948 Explosives with lined cavities. *J. Appl. Phys.* **19**, 563–582.

Bless, S. J., Barber, J. P., Bertke, R. S. & Swift, H. F. 1978 Penetration mechanics of yawed rods. *Intl J. Engng Sci.* **16**, 829–834.

Eichelberger, R. J. 1956 Experimental test of the theory of penetration by metallic jets. *J. Appl. Phys.* **27**, 63–68.

Golesworthy, R. C. 1983 The effect of transverse velocity on shaped charge performance. In *Proc. 7th Intl Symp. Ballistics, April, 1983, The Hague* pp. 257–260. The Hague: K.I.vI.

Golesworthy, R. C. & Townsend, I. 1984 Analytical model of shaped charge penetration in the direct and overflying top attack modes. In *Proc. 8th Intl Symp. Ballistics, October, 1984, Orlando,* Session VII pp. 1–14. Wilmington MA: AVCO Systems Division.

Held, M. 1984 Transverse shaped charges. In *Proc. 8th Intl Symp. Ballistics, October, 1984, Orlando,* Session VII pp. 39–47. Wilmington MA: AVCO Systems Division.

Held, M. & Fischer, R. 1986 Penetration theory for inclined and moving shaped charges. *Propellants, Explosives, Pyrotechnics* **11**, 115–122.

Hopkins, D. F. & Robertson, J. M. 1967 Two dimensional incompressible fluid jet penetration. *J. Fluid Mech.* **29**, 273–287.

Lighthill, J. 1979 A simple fluid-flow model of ground effect on hovering. *J. Fluid Mech.* **93**, 781–797.

Milne-Thomson, L. M. 1968 *Theoretical Hydrodynamics.* Macmillan.

Pack, D. C. & Evans, W. M. 1951 Penetration by high velocity jets. *Proc. Phys. Soc. Lond.* B **64**, 298–302.

Ravid, M., Bodner, S. R. & Holcman, I. 1987 Analysis of very high speed impact. *Intl J. Engng Sci.* **25**, 473–482.

Tate, A. 1967 A theory for the deceleration of long rods after impact. *J. Mech. Phys. Solids* **15**, 387–399.

Tate, A. 1986 Long rod penetration models – part II. Extensions to the hydrodynamic theory of penetration. *Intl J. Mech. Sci.* **28**, 599–612.